Power Differential Protection for Transformer Based on Fault Component Network

Fang Peng, *Member, IEEE*, Houlei Gao, Jiakai Huang, Yifei Guo, Yiqing Liu, and Yongfeng Zhang

***Abstract*—Current differential protection has been widely used as the primary protection of transformers. However, inrush currents during transformer energization can cause misoperation of the protection when the second harmonic restraint algorithm fails. This article proposes a power differential protection scheme based on the fault component network (FCN), which is free from inrush detection and computationally cheap. First, the fault component differential power (FCDP), defined as the differential active power of a transformer in the FCN, is analyzed under different conditions. Second, a transformer protection scheme is presented based on the FCDP and the traditional differential power. A removal algorithm of decaying direct current (DDC) offset is developed to accurately estimate the FCDP. The performance of the scheme is tested under various conditions, including internal faults, external faults and transformer energization. The simulations using PSCAD and Real Time Digital Simulator (RTDS), experiments in the Electrical Power Dynamic Laboratory (EPDL) and real recording data validate that the proposed method can protect the transformer reliably.**

***Index Terms*—Current differential protection, fault component, magnetizing inrush, power differential protection, power transformer.**

I. Introduction

CURRENT differential protection is generally used as the primary protection for transformers rated over 10 MVA [1], [2], [3]. Despite the good performance in discriminating between internal faults and external faults, the current differential protection may misoperate because of the magnetizing inrush [4], [5]. When a transformer is energized, the inrush is generated due to the fact that the flux linkage of iron core cannot abruptly change [6]. Second harmonic components are widely used for detecting inrush and blocking the differential relays [7], [8].

Manuscript received 5 July 2022; revised 13 October 2022 and 20 December 2022; accepted 15 January 2023. Date of publication 13 February 2023; date of current version 25 July 2023. This work was supported in part by the National Natural Science Foundation of China under Grant 51877127, and in part by Shandong Provincial Natural Science Foundation of China under Grant ZR2022ME097. Paper no. TPWRD-00997-2022. *(Corresponding author: Houlei Gao.)*

Fang Peng and Houlei Gao are with the Key Laboratory of Power System Intelligent Dispatch and Control of Ministry of Education, Shandong University, Jinan 250061, China (e-mail: pengfang@sdu.edu.cn; houleig@sdu.edu.cn).

Jiakai Huang is with the Electric Power Research Institute, State Grid Tianjin Electric Power Company, Tianjin 300384, China (e-mail: hjk1026@sina.cn).

Yifei Guo is with the School of Engineering, University of Aberdeen, Aberdeen AB24 3UE, U.K. (e-mail: yifei.guo@abdn.ac.uk).

Yiqing Liu and Yongfeng Zhang are with the School of Electrical Engineering, University of Jinan, Jinan 250022, China (e-mail: cse_liuyq@ujn.edu.cn; cse_zhangyf@ujn.edu.cn).

Color versions of one or more figures in this article are available at https://doi.org/10.1109/TPWRD.2023.3244535.

Digital Object Identifier 10.1109/TPWRD.2023.3244535

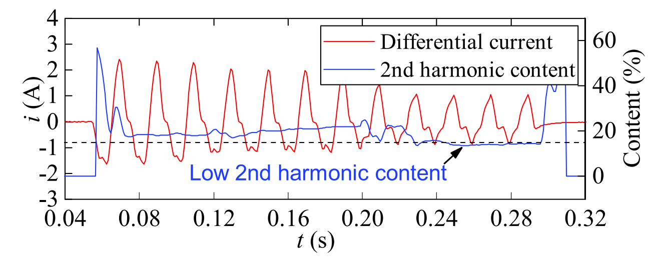

Fig. 1. Differential Current and Second Harmonic Component Recorded in the Field.

However, there may be a period of delay in protection operation due to second harmonic components of fault currents [9]. Particularly, the second harmonic components will increase if the transformer is connected to a long transmission line with a shunt reactor or series capacitor [10]. Thus, the relay may refuse to trip during internal faults. On the other hand, the detection of magnetizing inrush may fail, since the second harmonic components significantly decrease due to the ultra-saturation phenomenon, high-permeability material used in the transformer core, and application of three-winding ultra high voltage (UHV) autotransformer [11], [12]. Misoperations of transformer protection under inrush conditions have been reported [13]. As a result, extensive outages and blackouts will occur.

The real-world recording data from a substation in North China suggest that the second harmonic restraint method may fail under some circumstances. In this event, a YNyn0d11-type transformer (230/121/38.5 kV, 180/180/90 MVA) was under a normal condition before deenergization. The load was 40–60%, and it was deenergized due to the switchgear replacement. Regarding the protection design, if the second harmonic content of a single phase is above 15%, the differential protection of the phase will be blocked. As shown in Fig. 1, when the transformer is energized, the second harmonic component of the differential current falls below 15% (black dashed line) after $t = 0.24$ s, resulting in a false trip of the relay.

A number of artificial intelligence and signal processing techniques have been leveraged to identify the magnetizing inrush [14], such as artificial neutral network [16], fuzzy logic [17], wavelet transform [18], and mathematical morphology [10]. However, the neutral network and fuzzy logic techniques usually require large training datasets and long computation time [19]. They are not physically interpretable, and the training data are usually generated by simulations which may not well replicate the real fault characteristics of transfomers, leading to difficulties in practical application. The wavelet-based methods are sensible and effective, but they usually require a high sampling rate and could also be influenced by high-frequency signals [20]. The mathematical morphology-based methods are able to improve the accuracy and speed of inrush identification, whereas the difficulty in common threshold selection causes a few limitations [4]. Besides, [21] proposes a magnetization hysteresis-based protection algorithm with high reliability and efficiency. Reference [22] uses the superimposed differential current and extracts its positive and negative sequence components to discriminate internal faults. Reference [23] proposes an inrush identification method based on the ratio of absolute difference to absolute sum of current magnitudes at both transformer sides. Reference [24] proposes a setting-free algorithm using the second central moment value of instantaneous differential currents. However, the methods in [21], [22], [23], [24] are vulnerable under three-phase fault conditions. Several estimation-based methods are also proposed to predict the waveform during inrush [4], [25], but they require the complete knowledge of transformer parameters. Although techniques above provide alternatives or improvements to existing method, there is still a gap between theoretical research and practical deployment. Moreover, several aforementioned techniques distinguish inrush from faults based on the differential current, which is just the inrush current during energization; consequently, they are not immune against inrush in theory.

Owing to the nonlinear relationship between the voltage and current of the transformer core, transformers cannot be well characterized by current solely. Therefore, voltage can be introduced to improve the performance of the transformer protection. In [26], a power differential transformer protection is, for the first time, provided on the basis of energy conservation law, where the differential active power is calculated for fault detection [27]. The method can detect weak faults sensitively [28]. It is free from influence of the inrush, since transformers will primarily absorb the reactive power rather than the active power during inrush. Meanwhile, the power differential protection principle has been applied to line protection [29], [34]. The power differential protection methods based on the full steady-state and fault components are studied, respectively. The former is used to protect transmission lines in [29], [30], which presents good performance in synchronization error cases and has high sensitivity during high-impedance ground faults [31]. However, the differential power based on the full steady-state component may decrease to a very low level while a fault with small fault impedance occurs at the terminal of the protected element in that the voltage significantly drops, and the power cannot be calculated accurately. Therefore, the traditional power differential protection cannot distinguish between internal faults and external faults under such conditions.

The fault component can improve the sensitivity of the current differential protection [32] and deal with the challenges caused by low voltage, which has been applied to the power differential protection of transmission lines in [27], [33], [34]. To improve the fault identification speed, instantaneous differential power is further studied in [27]. Nonetheless, its effectiveness under the inrush condition remains an open question.

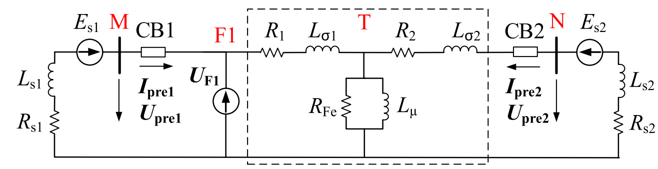

Fig. 2. Equivalent Prefault Network under the Normal Condition.

We propose a transformer protection scheme based on the energy conservation law and superposition principle in this paper. Differential power in the fault component network (FCN) and the full steady-state component network is utilized to develop two complementary criteria. A large voltage drop at the end of the transformer will not make the protection fail. Besides, the proposed scheme is immune to inrush; thereby, the inrush detection is no longer needed. With application in relays considered, the proposed algorithm is computationally cheap and therefore easy-to-implement in practice. Simulations using PSCAD and Real Time Digital Simulator (RTDS), experiments in the Electrical Power Dynamic Laboratory (EPDL) and recording data of an actual transformer demonstrate that the scheme is able to protect the transformer reliably under various conditions.

The rest of this paper is organized as follows. In Section II, the concept of fault component differential power (FCDP) is introduced. Section III presents the FCDP-based transformer protection scheme, including the main criterion, auxiliary criterion and the removal algorithm for decaying direct current (DDC) components. Section IV tests the proposed scheme under internal fault, external fault, and transformer energization conditions, followed by conclusions.

II. Differential Power in Fault Component Network

The FCDP is first defined in this section based on the energy conservation law and superposition principle. Then, the FCDPs under internal fault, external fault, and magnetizing inrush conditions are analyzed using the FCN. The FCDPs under different conditions are compared to develop the new transformer protection scheme.

A. Definition of Fault Component Differential Power

When a fault occurs, voltages and currents across the network will significantly change. The changes of voltages and currents are caused by the fault voltage source superimposed at the fault point. In accordance with the superposition principle, the whole faulted network is comprised of the prefault network and the FCN [35]. The prefault network and FCN containing a single-phase two-winding transformer are shown in Figs. 2 and 3, respectively. E_{s1} and E_{s2} are the system equivalent voltages at M terminal and N terminal; R_{s1}, R_{s2}, L_{s1}, and L_{s2} are the system equivalent resistances and inductances at the two terminals; R_1 and R_2 are the winding resistances of primary and secondary sides; $L_{\sigma 1}$ and $L_{\sigma 2}$ are the winding leakage inductances; R_{Fe} and L_μ denote the iron core loss resistance and the magnetizing

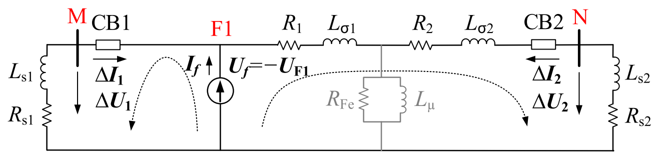

Fig. 3. Equivalent FCN During Internal Faults.

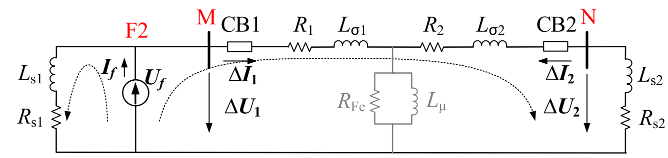

Fig. 4. Equivalent FCN During External Faults.

inductance. As shown in Fig. 2, a fault occurs at F1 which is within the protection zone of the transformer relay. U_{F1} is the prefault voltage at F1; U_{pre1} and U_{pre2} are the prefault voltages at buses M and N; I_{pre1} and I_{pre2} are the prefault currents flowing through CB1 and CB2, respectively. U_f is the superimposed voltage source in the FCN; I_f is the current flowing through the superimposed voltage source. ΔU_1, ΔU_2, ΔI_1, and ΔI_2 represent fault component voltages and currents.

The fault components can be calculated by,

$$\begin{cases}\Delta \boldsymbol{U}_1 = \boldsymbol{U}_{\mathrm{fault1}} - \boldsymbol{U}_{\mathrm{pre1}}\\ \Delta \boldsymbol{U}_2 = \boldsymbol{U}_{\mathrm{fault2}} - \boldsymbol{U}_{\mathrm{pre2}}\\ \Delta \boldsymbol{I}_1 = \boldsymbol{I}_{\mathrm{fault1}} - \boldsymbol{I}_{\mathrm{pre1}}\\ \Delta \boldsymbol{I}_2 = \boldsymbol{I}_{\mathrm{fault2}} - \boldsymbol{I}_{\mathrm{pre2}}\end{cases} \tag{1}$$

where U_{fault1} and U_{fault2} are respectively voltages at buses M and N under fault conditions. I_{fault1} and I_{fault2} are the currents in the CB1 and CB2 under fault conditions, respectively.

For digital relays, the fault components of the nth voltage and current samples can be calculated as,

$$\begin{cases}\Delta u(n) = u(n) - u(n-kN)\\ \Delta i(n) = i(n) - i(n-kN)\end{cases} \tag{2}$$

where k is a positive integer, and N is the number of the samples during one cycle.

The differential active power in FCN is called FCDP, which is the active power injected into the transformer from the ends. It can be calculated as,

$$\begin{aligned}\Delta P &= \Delta P_1 + \Delta P_2\\ &= \mathrm{Re}(\Delta \boldsymbol{U}_1 \cdot \Delta \boldsymbol{I}_1^*) + \mathrm{Re}(\Delta \boldsymbol{U}_2 \cdot \Delta \boldsymbol{I}_2^*)\\ &= |\Delta \boldsymbol{U}_1||\Delta \boldsymbol{I}_1| \cos(\varphi_{u1} - \varphi_{i1})\\ &\quad + |\Delta \boldsymbol{U}_2||\Delta \boldsymbol{I}_2| \cos(\varphi_{u2} - \varphi_{i2})\end{aligned} \tag{3}$$

where ΔP_1 and ΔP_2 are the power flowing into the primary and secondary sides of the transformer in the FCN; φ_{u1} and φ_{i1} are the phase angles of ΔU_1 and ΔI_1; φ_{u2} and φ_{i2} are the phase angles of ΔU_2 and ΔI_2, respectively.

Note that under normal conditions, there is no fault component voltage source; currents and voltages at both sides of the transformer will not change, implying that $\Delta P = 0$.

B. Internal Faults

As shown in Fig. 3, the fault component voltage source is superimposed between buses M and N during internal faults. The voltages at the two buses in the FCN are expressed as

$$\begin{cases}\Delta \boldsymbol{U}_1 = -\Delta \boldsymbol{I}_1(R_{\mathrm{S1}} + jX_{\mathrm{S1}})\\ \Delta \boldsymbol{U}_2 = -\Delta \boldsymbol{I}_2(R_{\mathrm{S2}} + jX_{\mathrm{S2}}).\end{cases} \tag{4}$$

Therefore, the FCDP is given by

$$\Delta P = -|\Delta \boldsymbol{I}_1|^2 R_{\mathrm{S1}} - |\Delta \boldsymbol{I}_2|^2 R_{\mathrm{S2}}. \tag{5}$$

It can be concluded that the FCDP during internal faults is negative and equal to the active power absorbed by the system resistance in the FCN.

The fault voltage source can deliver active power to both ends of the transformer, while the winding resistances absorb the active power. Since the magnetizing impedance is large, the magnetizing branch can be ignored. As a result, the FCDP can also be expressed as

$$\Delta P = -|\Delta \boldsymbol{I}_2|^2 (R_1 + R_2) - \mathrm{Re}(\boldsymbol{U}_f \cdot \boldsymbol{I}_f^*). \tag{6}$$

Given that the winding resistance is small, the active power flowing through the transformer is also small. In contrast, the active power delivered from the fault voltage source is much larger. Therefore, the negative polarity of the FCDP can be confirmed.

C. External Faults

As shown in Fig. 4, an external fault occurs at F2 where a fault component voltage source is superimposed. Ignoring the magnetizing branch of the transformer, the currents flowing through CB1 and CB2 are

$$\Delta \boldsymbol{I}_1 = -\Delta \boldsymbol{I}_2 = \frac{\Delta \boldsymbol{U}_1 - \Delta \boldsymbol{U}_2}{(R_1 + R_2) + j(X_{\sigma1} + X_{\sigma2})}. \tag{7}$$

Then, the FCDP can be expressed as

$$\begin{aligned}\Delta P &= \mathrm{Re}(\Delta \boldsymbol{U}_1 \cdot \Delta \boldsymbol{I}_1^* + \Delta \boldsymbol{U}_2 \cdot \Delta \boldsymbol{I}_2^*)\\ &= \mathrm{Re}(\Delta \boldsymbol{U}_1 - \Delta \boldsymbol{U}_2) \cdot \Delta \boldsymbol{I}_1^*\\ &= \mathrm{Re}\{\Delta \boldsymbol{I}_1 \cdot \Delta \boldsymbol{I}_1^* [(R_1 + R_2) + j(X_{\sigma1} + X_{\sigma2})]\}\\ &= |\Delta \boldsymbol{I}_1|^2 (R_1 + R_2).\end{aligned} \tag{8}$$

It can be observed from (8) that the FCDP is the active power absorbed by the winding resistances. The FCDP during the external fault is positive; hence, it has an opposite polarity to the FCDP during the internal fault. In general, the winding resistance is much smaller than the system resistance. This indicates that the FCDP during external faults is much smaller than that during internal faults.

D. Magnetizing Inrush

Magnetizing inrush is generated when an unloaded transformer is switched on, which can be treated as a current source superimposed at the magnetizing branch (see Fig. 5).

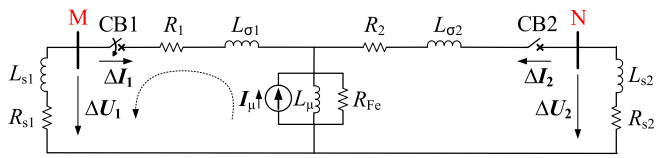

Fig. 5. Equivalent FCN During Magnetizing Inrush.

When inrush occurs, the inductance in the circuit changes nonlinearly, while the superposition principle is applied in the linear system. Thus, the FCDP during inrush is calculated using the definition as per (3) rather than (5). A temporary voltage drop will occur during the inrush. Since the transformer is unloaded, the FCDP only consists of the power at the primary terminal, i.e.,

$$\Delta P = \mathrm{Re}(\Delta \boldsymbol{U}_1 \cdot \Delta \boldsymbol{I}_1^*) = \alpha |\boldsymbol{U}_{\mathrm{N}1}| \cdot \beta |\boldsymbol{I}_{\mathrm{N}1}| \cdot \cos(\varphi_{u1} - \varphi_{i1}), \tag{9}$$

where α is the proportion of the decreased voltage to the rated phase voltage $\boldsymbol{U}_{\mathrm{N}1}$; β is the proportion of the increased current to the rated phase current $\boldsymbol{I}_{\mathrm{N}1}$. $\varphi_{u1} - \varphi_{i1}$ is close to $180^\circ - \delta$, where δ is the phase angle of the system impedance.

Since the current increases and the voltage decreases, the FCDP during inrush is negative. However, the FCDP is not as large as that during the internal fault. The voltage decrease is the key for distinguishing between the internal fault and inrush. The maximum voltage decrease ratio α of a transformer during inrush can be calculated as

$$\alpha_{\max}^{\mathrm{inrush}} = X_{\mathrm{S}}/(X_{\mathrm{S}} + 2.5X_{\mathrm{T}}), \tag{10}$$

where X_{S} is the system reactance, and X_{T} is the transformer leakage reactance [36]. In comparison, α during internals fault (α^{fault}) can be calculated according to Fig. 3. When the fault locates at the end of the secondary side, the voltage drop can be calculated as follows. $\boldsymbol{U}_f$ is at the right side of the transformer. Before the fault occurs, the voltage across the system impedance and the transformer impedance can be ignored, i.e., $U_f \approx U_N$. $\alpha^{\mathrm{fault}} = \Delta U/U_f = X_{\mathrm{S}}/(X_{\mathrm{S}} + X_{\mathrm{T}})$ can be obtained. It is clearly seen that the maximum voltage drop at the primary side caused by the inrush current is less than the voltage drop during faults. If the fault locates at the terminal of the primary side, the statement will also be true. In addition, a larger voltage drop due to inrush will occur in a weaker system while the inrush current is much smaller. This motivates us to distinguish between internal faults and magnetizing inrush by setting a threshold of the FCDP.

III. Proposed Protection Scheme Based on the Fault Component Network

In this section, a transformer protection scheme is proposed on the basis of the FCN. The scheme consists of the main criterion (FCDP-based criterion) and auxiliary criterion.

A. FCDP-Based Criterion

As analyzed in Section II, internal faults can be identified by the polarity and value of FCDP. Under normal and external fault conditions, the FCDP is positive and very small, since it is the active power absorbed by the transformer, i.e., the power consumed by winding resistance. Under internal fault conditions, the FCDP is negative and large, since the active power delivered from the fault component voltage source is large. Accordingly, the FCDP-based criterion for detecting internal faults is given by,

$$\begin{cases} \Delta P = \sum\limits_{j \in \mathcal{J}} \sum\limits_{i \in \mathcal{I}} \mathrm{Re}(\Delta \boldsymbol{U}_{ij} \cdot \Delta \boldsymbol{I}_{ij}^*) < 0 \\ |\Delta P| > P_{\mathrm{fset}}. \end{cases} \tag{11}$$

The set $\mathcal{I} := \{1, 2, 3\}$ represents the primary, secondary, and tertiary (if any) side of the transformer, respectively. The set $\mathcal{J} := \{\mathrm{A}, \mathrm{B}, \mathrm{C}\}$ represents the phase.

The threshold P_{fset} is set to prevent the protection from misoperation due to the inrush current. Its value of each phase is set as (12), and the sum of the three-phase values is used in (11).

$$P_{\mathrm{fset}j} = \begin{cases} \dfrac{K_{\mathrm{rel1}} X_{\mathrm{S}}}{X_{\mathrm{S}} + 2.5X_{\mathrm{T}}} |\boldsymbol{U}_{\mathbf{N1}}| \cdot |\Delta \boldsymbol{I}_1| \cos\varphi_d & \Delta P < 0 \\ 0 & \Delta P > 0 \end{cases}, \tag{12}$$

where $\varphi_d = \varphi_{u1} - \varphi_{i1}$. K_{rel} is the coefficient of reliability and taken as $1\sim1.5$, empirically. Furthermore, the maximum inrush current is limited by the transformer capacity which can be $4\sim8$ times of the rated current. Meanwhile, φ_d is approximately equal to $180^\circ - \delta$. As such, the maximum threshold is

$$P_{\mathrm{fset}j}^{\max} = \frac{K_{\mathrm{rel1}} \beta_{\max} X_{\mathrm{S}}}{X_{\mathrm{S}} + 2.5X_{\mathrm{T}}} |\boldsymbol{U}_{\mathbf{N1}}| \cdot |\Delta \boldsymbol{I}_1| \cos\delta. \tag{13}$$

$\beta_{\max}$ of different transformer capacities is accessible in references [37]. If the transformer parameters change, the threshold value will be recalculated.

As presented in (13), the calculation of P_{fset} depends on the acquisition of system reactance and winding reactance. If the system reactance cannot be obtained accurately, the estimated maximum system impedance magnitude and minimum impedance angle at the corresponding voltage level can be used to calculate the maximum threshold. For a system with a certain voltage level, the system impedance varies within a fixed range. Taking the power grids of Shandong Province as an example, the equivalent impedance of 110 kV, 220 kV, and 500 kV systems varies within 4 Ω–35 Ω, 4 Ω–25 Ω, and 4 Ω–15 Ω, respectively. On the other hand, the transformer reactance may change with the aging of the transformer due primarily to winding deformation. The short-circuit impedance of the transformer is tested periodically to evaluate its performance [38]. The offline test value above can be used to determine the threshold in the main criterion, for the aging transformer. Although the difference between the actual value and offline test value may cause errors in estimation of the maximum voltage decrease, a larger K_{rel1} can be taken under this condition. Furthermore, the system impedance and transformer reactance can be obtained accurately in real time [39], [40], with the development and application of online monitoring technology for transformers, which will help resolve the problems.

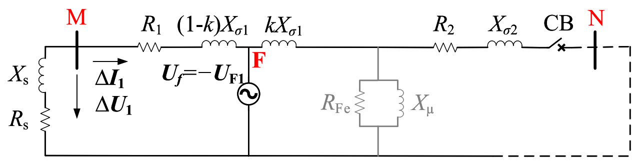

Fig. 6. FCN under Energization with an Internal Fault condition.

B. Protected Area of the FCDP-Based Criterion for Windings

If the internal fault does not occur at the terminal, $\alpha_{\max}^{\text{inrush}} < \alpha^{\text{fault}}$ may not be true. Thus, the protected area of the FCDP-based criterion for the windings should be discussed.

If a metallic fault occurs at the k percentage of the primary windings, the simplified circuit can be presented as Fig. 6, where $U_f \approx kU_N$. Then, it follows that

$$\alpha^{\text{fault}} = \frac{kX_{\text{S}}}{X_{\text{S}} + \dfrac{(1-k)}{2}X_{\text{T}}}. \tag{14}$$

Based on (10) and (14), $\alpha_{\max}^{\text{inrush}} < \alpha^{\text{fault}}$ will not be true if k is low. Considering the typical ranges of the winding reactance (20–40 Ω) and system reactance (4–40 Ω), if $k < 25\%$, $\alpha_{\max}^{\text{inrush}} > \alpha^{\text{fault}}$, and consequently the protection may fail. In other words, 75% of the windings can be protected by the main criterion when the metallic winding-to-ground fault occurs during energization.

Energization with the secondary winding breaker open is the most challenging condition for the main criterion, but in fact, transformers are in service for most of the time. When the fault occurs, the voltage and current at the terminal of the secondary winding will also change. They can contribute a lot to the FCDP, especially if the secondary winding is connected to the load only.

C. Auxiliary Criterion

The threshold of P_{fset} in the main criterion results in low protection sensitivity under the high fault impedance condition. The same thing happens to a turn-to-turn fault with a small short-circuit turn ratio. To increase the protection sensitivity, an auxiliary criterion is proposed using conventional differential active power P_{d} (based on the full steady-state component). The fault impedance is mainly resistive. Differential power flowing into the transformer is:

$$P_{\text{sum}} = \sum_j \sum_i \left(|\boldsymbol{I}_{ij}|^2 \cdot R_i\right) + \sum_j \left(\sum_i \left(|\boldsymbol{I}_{ij}|^2\right) \cdot R_f\right). \tag{15}$$

In comparison, the magnetizing branch works as an inductance during inrush. Therefore, the transformer mainly consumes active power rather than reactive power during faults, and it mainly absorbs reactive power during inrush. Thus, the differential power can be used to distinguish inrush from internal faults. The auxiliary criterion is given as:

$$P_{\text{d}} = \sum_j \sum_i \left(\text{Re}(\boldsymbol{U}_{ij} \cdot \boldsymbol{I}_{ij}^*) - |\boldsymbol{I}_{ij}|^2 \cdot R_i\right) > P_{\text{set}}. \tag{16}$$

Note that the auxiliary criterion is also based on the energy conservation law. In (16), the active power consumed by the winding resistance is subtracted to calculate the active power consumed by the fault resistance. The P_{set} is used to prevent the influence of the measuring error and calculation error during inrush or external faults. The threshold can be set as 0.08∼0.1 p.u., typically. Furthermore, when the voltage drops greatly, a large calculation error in P_{d} may occur. Thus, the auxiliary criterion is used only if the voltage drop ratio of each phase is less than the threshold U_{set}, and it works one cycle later after the protection starts up. U_{set} is taken as $K_{\text{rel1}}K_{\text{rel2}}\alpha_{\max}^{\text{inrush}}$, where K_{rel2} is 1.5∼2. When the voltage drop is small, the conventional differential power can reflect internal faults sensitively.

D. Removal of the DDC Offset

Accurate calculation of the differential power depends on the accurate estimation of the fundamental components. The DFT filter can remove the constant direct current (DC) component and harmonics. However, the DDC component could not be filtered out, and it can lead to oscillations in the magnitude and phase angle of the fundamental component.

Furthermore, the FCDP value is calculated using the phase angle difference between $\Delta\boldsymbol{U}$ and $\Delta\boldsymbol{I}$, namely the system impedance angle δ. It is usually close to 90° [41] and thus, a small error in the phase angle will lead to a large error in the power value.

To remove the DDC component, a differential filter is utilized for the DFT. The full current signal including the DDC component is

$$x(t) = X_0 e^{-t/\tau} + \sum_{k=1}^{\infty} X_{\text{m}k} \sin(k\omega t + \varphi_k). \tag{17}$$

Assume the DDC component is constant in a very short instant, i.e., it can be removed by two sampled values of x. Then, a new variable is given as

$$\begin{aligned} y(n) &= x(n) - x(n-M) \\ &= \sum_{k=1}^{\infty} X_{\text{m}k}\{\sin(k\omega T_{\text{s}}n + \varphi_k) - \sin[k\omega T_{\text{s}}(n-M) + \varphi_k]\} \end{aligned} \tag{18}$$

where $M \geqslant 1$ is the step size; T_s is the sampling interval.

Define the fundamental component of $y(t)$ as $y_1(t) = Y_{\text{m1}}\sin(\omega t + \theta_1)$. Y_{m1} and θ_1 can be calculated by the DFT algorithm. Then, the magnitude and phase angle of x_1 are

$$\begin{cases} X_{\text{m1}} = \dfrac{Y_{\text{m1}}}{2\sin\dfrac{\omega T_{\text{s}}M}{2}} \\ \varphi_1 = \theta_1 - \dfrac{\pi}{2} + \dfrac{\omega T_{\text{s}}M}{2}. \end{cases} \tag{19}$$

As a result, the DDC component can be removed, and more accurate fundamental phasor can be captured.

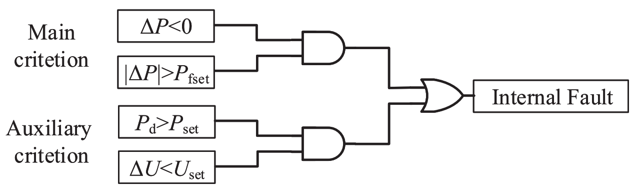

Fig. 7. Logical Block Diagram of the FCDP-Based Scheme.

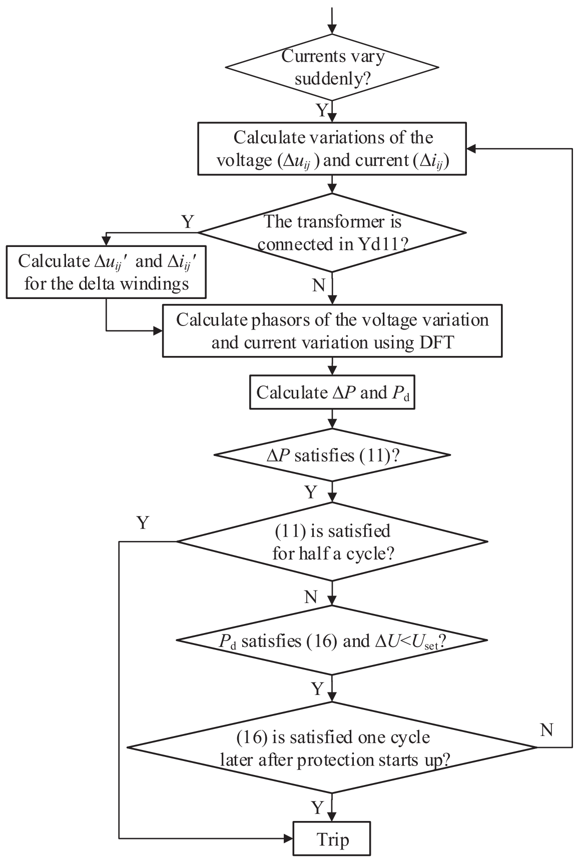

Fig. 8. Flowchart of the FCDP-based Scheme.

E. Proposed Scheme

Fig. 7 shows the logical block diagram of the proposed scheme. The main criterion uses the fault components of voltages and currents, while the auxiliary criterion uses the full steady-state components. The action of the main criterion depends on the polarity and value of the FCDP, while the trip of the auxiliary criterion depends on the voltage drop and power value consumed by the transformer. A large voltage drop is more favorable for the main criterion, while a relatively low voltage drop is more favorable for the auxiliary criterion. The two criteria can complement each other under different conditions. There is an intersection between the protection areas of the two criteria.

Fig. 8 shows the flowchart of the proposed protection scheme. The FCDP-based algorithm is triggered when a sudden change in currents is detected. Then, the variations of voltage and current are calculated. If the transformer is a Yd11 transformer, new voltages and currents are calculated by Y-Δ transformation.

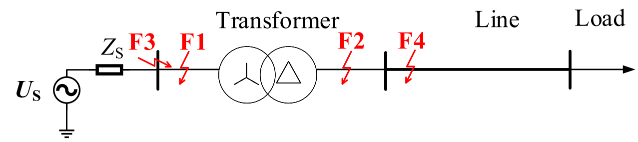

Fig. 9. Simulation Model.

TABLE I
PARAMETERS OF THE SIMULATION MODEL

Parameter	Value	Parameter	Value
U_{S}	$220\angle 0^{\circ}$ kV	Winding connection	Yd11
f	50 Hz	Knee Voltage	1.15 p.u.
Z_{S}	$20\angle 85^{\circ}$ Ω	Copper losses	0.0032 p.u.
S_{N} (Rated capacity)	120 MVA	x_T (Positive leakage reactance)	0.10 p.u.
$U_{1\mathrm{N}}/U_{2\mathrm{N}}$	220 kV/ 38.5 kV	Load	90+j10 MVA

Traditional DFT is used to obtain the voltage phasor, and the differential DFT is used to obtain the current phasor. Then, ΔP and P_d are calculated, and (11) or (16) is judged. Note that the differential DFT algorithm is only applied to the current signal, since there is no DDC component in the voltage signal, and this algorithm will amplify high-frequency components. To reduce the influence of high-frequency components and other interferences on the power value, the trip signal will be sent only when the criterion is satisfied for half a cycle. The half-cycle delay can help improve the reliability of the protection. In addition, the voltage for calculation can be obtain from the voltage transformer (VT) of the bus.

IV. PERFORMANCE EVALUATION

The proposed scheme is tested under internal fault, external fault, and transformer energization conditions in this section. The system model including a transformer is developed under PSCAD/EMTDC and RTDS environment. Here, RTDS is utilized to simulate turn-to-turn faults and turn-to-ground faults. Experimental tests are performed in the EPDL for further investigation. Recording data of an actual power transformer are also used to validate the performance during inrush. Resultant voltages and currents are loaded into Matlab to implement the protection algorithm.

A. Internal Faults

Fig. 9 shows the simulation model constructed in PSCAD. U_{S} and Z_{S} represents the equivalent model of the power system connected with the transformer. The transformer parameters listed in Table I can be conveniently obtained by the transformer nameplate, which can be used to calculated the threshold of the proposed scheme. The winding leakage reactance can be calculated approximately as (20). The system frequency is 50 Hz, and the sampling rate is 4000 Hz. For a 120 MVA transformer, the maximum inrush current is five times of the rated current, i.e., $\beta_{\max} = 5$ [37]. The system impedance is taken as 20Ω and δ is 85°. The X/R ratio ρ is 11.4. X_{T} is calculated based on the rated

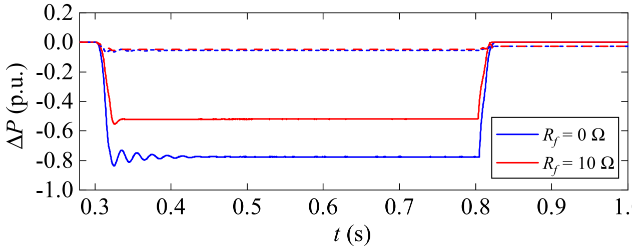

Fig. 10. FCDP During Internal Phase A-to-ground faults.

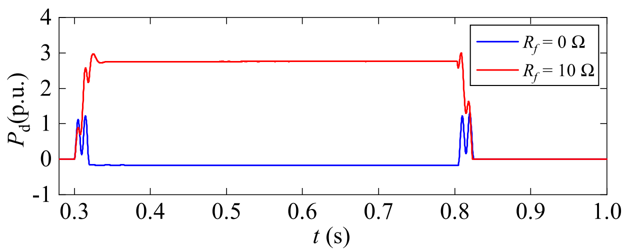

Fig. 11. Traditional Differential Power During Phase A-to-ground Faults.

impedance. Therefore, $\alpha_{\max}^{\text{inrush}}$ is 0.17 and $P_{\text{fset}}^{\max}$ is 3.46 MW (0.0288 p.u.) for each phase as per (12) and (13) when K_{rel} is 1.1.

$$X_{\text{T}} = x_{\text{T}} \cdot Z_{\text{N}} = x_{\text{T}} \frac{U_{1\text{N}}^2}{S_{\text{N}}}. \tag{20}$$

The proposed scheme is then validated under an internal fault condition. The faults occur at $t = 0.3$ s and last for 0.5 s. The waveforms of ΔP during AG faults at F1 are shown in Fig. 10. Power values under $R_{\text{f}} = 0\ \Omega$ and $10\ \Omega$ conditions exceed the threshold (represented by the dashed line) at $t = 0.30375$ s and $t = 0.30425$ s, respectively. The internal faults can be detected successfully. The performance of traditional power differential protection is also tested for comparison. The whole components of voltages and currents are utilized instead of fault components. As shown in Fig. 11, the traditional differential power is as low as 0 MW after $t = 0.32$ s under the condition of $R_{\text{f}} = 0\ \Omega$, in which case the internal fault fails to be detected.

Different types of faults at F1 and F2 are simulated for further evaluation of the proposed scheme. Tables II and III list the FCDPs of each phase and the sum during the faults at F1 and F2, respectively. Transformation of Y$-\Delta$ is applied in the voltage and current for ΔP_j. Δt_{op} represents the time from fault occurrence to the instant that the FCDP exceeds the threshold. When a single-phase-to-ground fault occurs at the delta side of the transformer, the fault current fails to flow through the circuit loop. Thus, the AG fault is not simulated.

It can be seen from the tables that internal faults can be successfully detected in 1/2 cycle after the fault occurs in above cases. In addition, the differential power values calculated by the conventional power differential method are also listed. The method fails when $R_{\text{f}} = 0\ \Omega$, while the FCDP-based method works effectively. The reason is that the voltages decrease to zero, and thus the differential power values cannot be estimated accurately. In comparison, the large variation of the voltage will lead to a large FCDP. Table IV lists the voltage and power based on the full steady-state component and fault component during a three-phase fault at F1, which clearly presents that the voltage drop causes a small value of P_1 and a large value of ΔP_1.

The conventional power differential method can be a complement of the FCDP-based method and improve protection sensitivity when faults with high fault impedance or turn-to-turn faults occur, especially at the low-voltage delta windings. Turn-to-turn faults and turn-to-ground faults are simulated by RTDS, where a precise transformer winding model with internal faults is included. The parameters are the same as those of the PSCAD model. The simulation results are listed in Tables V and VI. The short-circuit location represents the distance from the neutral point to the fault location. The FCDP-based method can identify most of the faults correctly, except the 5% turn-to-turn faults, while sensitivity of the auxiliary criterion is high. The voltage drop under this condition is low, and thus the proposed scheme can detect the fault reliably.

TABLE II
SIMULATION RESULTS DURING INTERNAL FAULTS AT F1

Fault Type	R_f (Ω)	ΔP (p.u.)	P_{fset} (p.u.)	ΔP_{A} (p.u.)	ΔP_{B} (p.u.)	ΔP_{C} (p.u.)	P_{d} (p.u.)	Δt_{op} (ms)
AG	0	−0.84	−0.06	−0.77	−0.04	−0.03	**−0.17**	3.75
	10	−0.55	−0.05	−0.51	−0.02	−0.02	2.76	4.25
AB	0	−1.28	−0.05	−0.63	−0.65	0.00	**−0.27**	2.75
	5	−1.24	−0.05	−0.61	−0.63	0.00	0.94	2.75
ABG	0	−1.64	−0.07	−0.81	−0.82	−0.04	**−0.35**	2.25
	5	−1.43	−0.07	−0.75	−0.68	−0.04	3.07	0.25
ABC	0	−2.47	−0.08	−0.87	−0.82	−0.85	**−0.55**	2.25

The bold entities indicate the best-performing results.

TABLE III
SIMULATION RESULTS DURING INTERNAL FAULTS AT F2

Fault Type	R_f (Ω)	ΔP (p.u.)	P_{fset} (p.u.)	ΔP_{A} (p.u.)	ΔP_{B} (p.u.)	ΔP_{C} (p.u.)	P_{d} (p.u.)	Δt_{op} (ms)
AB	0	−0.35	−0.07	−0.06	−0.23	−0.06	**0.05**	2.75
	5	−0.09	−0.03	−0.02	−0.06	−0.02	1.32	2.75
ABG	0	−0.35	−0.07	−0.06	−0.23	−0.06	**0.05**	2.75
	5	−0.03	−0.02	−0.01	−0.02	−0.01	0.9	3.00
ABC	0	−0.69	−0.08	−0.24	−0.23	−0.23	**0.09**	2.75

The bold entities indicate the best-performing results.

TABLE IV
COMPARISON OF THE TRADITIONAL POWER AND THE FCDP DURING A THREE-PHASE FAULT AT F1

	U(p.u.)	ΔU(p.u.)	P_1(p.u.)	P_d(p.u.)	ΔP_1(p.u.)	ΔP(p.u.)
Single Phase	0.03	-0.97	0.03	-1.04	-0.68	-0.85
Total	–	–	0.09	-0.55	-1.97	-2.47

TABLE V
SIMULATION RESULTS DURING TURN-TO-TURN FAULTS

Phase	A			B		
Short-circuit turn ratio	5%	10%	15%	5%	10%	15%
ΔP(p.u.)	−0.0023	−0.0310	−0.1073	−0.0035	−0.0385	−0.1142
P_{fset}(p.u.)	−0.0067	−0.0246	−0.0409	−0.0083	−0.0283	−0.0420
P_{d}(p.u.)	0.27	0.94	1.45	0.28	0.94	1.45
Δt_{op}(ms)	20.00	16.75	10.50	20.00	16.50	8.75

TABLE VI
SIMULATION RESULTS DURING TURN-TO-GROUND FAULTS

Short-circuit location	90%	70%	50%	30%	10%
ΔI(p.u.)	13.34	10.27	6.19	5.84	5.86
ΔP(p.u.)	−0.8441	−0.4541	−0.1748	−0.2247	−0.3022
P_{fset}(p.u.)	−0.0358	−0.0253	−0.0336	−0.0465	−0.0516
P_{d}(p.u.)	−0.12	−0.02	0.03	0.15	1.3
Δt_{op}(ms)	4.00	5.00	7.00	6.25	6.5

TABLE VII
SIMULATION RESULTS DURING EXTERNAL FAULTS AT THE BUS (F3) AND THE TRANSMISSION LINE (F4)

Fault Location	Fault Type	$R_f(\Omega)$	ΔP(p.u.)	P_{d}(p.u.)
F3	AG	0	0.03	**0.01**
		20	0.01	0.01
	AB	0	0.00	**0.00**
		5	0.00	0.00
	ABG	0	0.03	**0.02**
		5	0.03	0.01
	ABC	0	0.01	**0.00**
F4	AB	0	0.24	**0.19**
		5	0.06	0.07
	ABG	0	0.24	**0.18**
		5	0.02	0.03
	ABC	0	0.47	**0.37**

The bold entities indicate the best-performing results.

B. External Faults

For external faults at the bus (F3) and the transmission line (F4), the proposed scheme is also examined. As given in Table VII, the FCDPs are positive during external faults. (11) and (16) are not satisfied. Since the voltage variation is large during severe faults, the FCDP is calculated accurately and will not cause false trips. Fig. 12 shows the waveforms of FCDPs under AG faults at F3. It can be concluded that the proposed scheme is reliable during external faults.

The performance of the traditional power differential protection is also evaluated without the $\Delta U < U_{\mathrm{set}}$ criterion. P_{d} during internal and external faults is listed in Tables II, III, and VII in red and bold, which is always at a very low level and makes the fault detection difficult. During external faults, it may be larger than that during internal faults; thus, the traditional power differential protection cannot distinguish internal faults from external faults under the metallic fault conditions. It should be noted that the power values are negative during the F1 fault since the power consumed by the transformer cannot be obtained correctly due to the low voltage. In theory, they should be positive. Further, if the voltage at the bus drops greatly under faults with low impedance and other conditions, the reliability of the traditional power differential protection will be low. The $\Delta U < U_{\mathrm{set}}$ criterion enables that the auxiliary criterion is only used when the voltage drop is low, which can ensure the reliability of the protection.

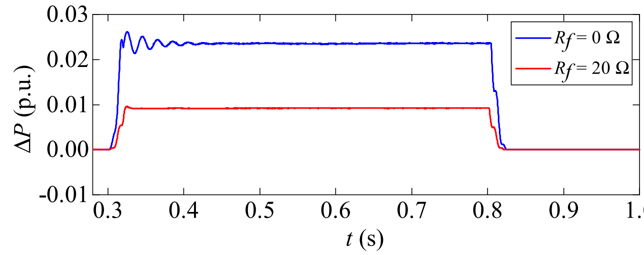

Fig. 12. FCDP During Phase A-to-ground Faults at F3.

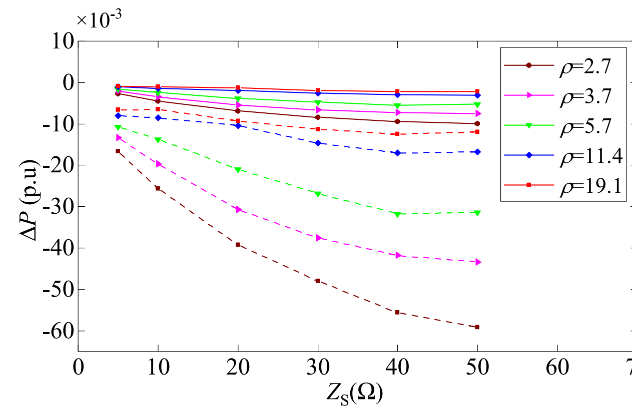

Fig. 13. FCDP During Energization Inrush.

C. Energization

Unloaded transformer energization cases are studied in this part. The transformer is energized with no fault at $t = 0.3$ s. The FCDP and P_{fset} are both negative and will reach the maximum absolute value at the instant of maximum inrush. Different system impedance and X/R ratio conditions are simulated in the energization cases, as shown in Fig. 13. The X/R ratio varies from 2.7 to 19.1 when the system impedance angle varies from 70° to 87°. The FCDP vaules shown in the figure are the ones whose magnitudes are the largest during inrush. Dashed lines in the figure represent the P_{fset} values. The protection will not operate falsely, since the FCDP does not exceed the threshold value. The system impedance magnitude and X/R ratio are critical factors that affect the threshold of FCDP. The inrush current decreases as the impedance increases and the X/R ratio decreases, while the voltage drops more greatly. The FCDP has the largest magnitude when $Z_S = 50\ \Omega$ and $\rho = 2.7$. Accurate magnitude and angle of the system impedance can help better

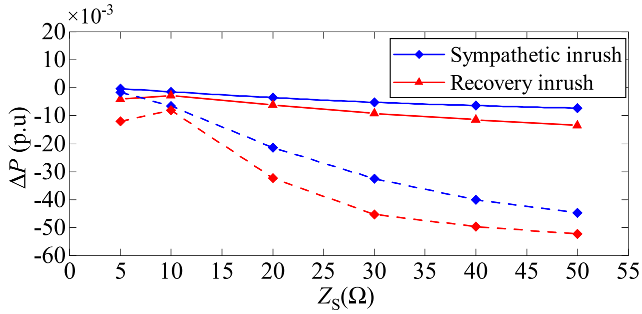

Fig. 14. FCDP During Sympathetic Inrush and Recovery Inrush.

detect faults by the main criterion. If there is none, the estimated maximum magnitude and minimum angle have to be used, which decreases the sensitivity of the main criterion due to a large P_{fset}. The different iron losses from 0.005 p.u. to 0.025 p.u. are used for the energized transformer in the cases as well, whereas the iron loss has little influence on the FCDP. There is little increment in the FCDP as the iron loss increases. The rationale behind this is that the iron loss is relevant to frequency, area of hysteresis loop, and flux density of the alternate flux, and the variation of the iron loss can hardly affect the inrush and the voltage drop.

Sympathetic inrush and recovery inrush cases under different impedances are simulated. The dashed line is the threshold of the main criterion. The largest FCDP magnitude is shown in Fig. 14. Compared with the energization inrush, the sympathetic inrush is less under the same condition. The voltage drop during inrush is caused by the parallel energizing transformer, and the influence of the maximum FCDP during inrush has been avoided by the threshold, thus the protection will not misoperate. The figure also shows that the recovery inrush will not cause false trips of the protection. The FCDPs are below the P_{fset} for the same reason. It should be noted that the protection starts up once the external fault occurs, and the voltages and currents under normal condition are recorded and used to calculate U_{pre} and I_{pre}.

Energization with an internal fault is simulated to compare with the inrush case. When the transformer is energized with the internal fault, the voltage and current of the secondary side are both zeros and thus ΔP_2 is zero, which is the most unfavorable condition for the main criterion. To compare the voltage drop and FCDP with the same benchmark, the two conditions are simulated at the same current increment level. The simulation results are listed in Table VIII. The fault type is the Phase A-to-ground fault at the primary side. The high inrush currents are obtained by setting high residual flux and low knee voltage; the data in the table are all the maximum magnitude during energization. The same fault current ΔI is simulated by setting high fault impedance. As seen in Table VIII, when the currents during faults are equal to the maximum inrush current, the voltage drop caused by the former is larger than that caused by the latter. The protection will not operate falsely. It should also be noted that the sensitivity decreases as the system impedance increases. The performance of the proposed method is also verified under the energization with turn faults condition, as listed in the Tables IX and X. $\alpha_{\max}^{\text{inrush}}$ is 0.16 p.u. The FCDP can work effectively when the short-circuit point varies from 10% to 50% of the windings during turn-to-ground faults, and the short-circuit ratio varies from 15% to 40% of the windings during turn-to-turn faults.

TABLE VIII
PERFORMANCE COMPARISON BETWEEN THE INRUSH AND ENERGIZATION WITH INTERNAL FAULTS CONDITIONS

$Z_S(\Omega)$		5	10	20	30
$R_f(\Omega)$		71	72	74	76
ΔI_A (p.u.)		5.4	5.1	4.6	4.2
ΔU_A (p.u.)	Inrush	0.0385	0.0749	0.1376	0.1898
	Fault	0.0667	0.1261	0.2277	0.3106
ΔP (p.u.)	Inrush	−0.0077	−0.0120	−0.0185	−0.0228
	Fault	−0.0107	−0.0188	−0.0309	−0.0392
P_{fset} (p.u.)	Inrush	−0.0139	−0.0226	−0.0340	−0.0417
	Fault	−0.0075	−0.0147	−0.0283	−0.0390
P_{d} (p.u.)	Inrush	0.0372	0.0419	0.0480	0.0520
	Fault	1.8380	1.7751	1.6373	1.4971

TABLE IX
SIMULATION RESULTS UNDER ENERGIZATION WITH TURN-TO-GROUND FAULTS CONDITION

Short-circuit location	10%	20%	30%	40%	50%
ΔI(p.u.)	6.17	6.26	5.84	5.56	6.61
ΔU_{A}(p.u.)	0.41	0.43	0.40	0.41	0.47
ΔP(p.u.)	−0.0953	−0.0988	−0.0872	−0.0848	−0.1091
P_{fset}(p.u.)	−0.0469	−0.0464	−0.0436	−0.0402	−0.0364
P_{d}(p.u.)	1.44	0.44	0.16	0.06	0.03

TABLE X
SIMULATION RESULTS UNDER ENERGIZATION WITH TURN-TO-TURN FAULTS CONDITION

Short-circuit ratio	15%	20%	25%	30%	40%
ΔI(p.u.)	3.56	4.67	4.99	4.96	4.27
ΔU_{A}(p.u.)	0.26	0.32	0.33	0.32	0.28
ΔP(p.u.)	−0.0330	−0.0539	−0.0611	−0.0593	−0.0433
P_{fset}(p.u.)	−0.0319	−0.0425	−0.0443	−0.0447	−0.0408
P_{d}(p.u.)	1.65	1.61	1.2	0.79	0.33

Here, the proposed main criterion is compared to the conventional current differential protection. Considering the second harmonic restraint method may fail to identify inrush, a threshold for the the current differential protection is set to mitigate the effect of inrush. Thus, $I_{\text{set}} = K_{\text{rel}}\beta_{\max}I_{\text{N}}$. Assume $K_{\text{rel}} = 1.2$ and $\beta_{\max} = 5$. I_{set} is 6 p.u. It is obvious that the current differential protection cannot work under the conditions in Table VIII. The current differential protection provides less complementarity than the FCDP-based criterion for the auxiliary protection. The red ΔI_{A} in Tables IX and X show that the current differential protection is unable to identify the faults in the corresponding situations. It should be noted that P_{d} is also too low to work when $k = 40\%$, which means only the FCDP-based criterion can identify the fault.

TABLE XI
SIMULATION RESULTS UNDER DIFFERENT RESIDUAL FLUX CONDITIONS

Residual Flux	0.2	0.4	0.6	0.8
2nd harmonic content of I_{dA}	0.2947	0.2271	0.1621	0.1118
2nd harmonic content of $I_{1\mathrm{A}}$	0.3806	0.2844	0.1965	0.1265
ΔU_A(p.u.)	0.0283	0.0353	0.0409	0.0460
ΔP(p.u.)	−0.0037	−0.0053	−0.0071	−0.0086
P_{fset}(p.u.)	−0.0101	−0.0105	−0.0114	−0.0117
P_{d}(p.u.)	0.0073	0.0075	0.0067	0.0084

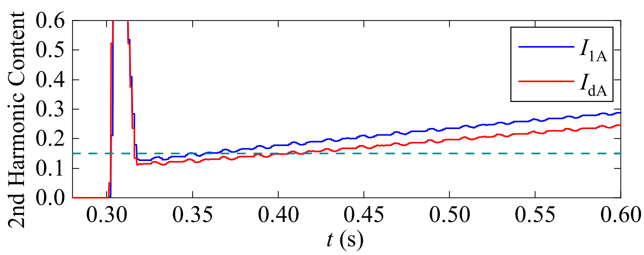

Fig. 15. Second Harmonic Content During Ultra-Saturation.

D. Ultra-Saturation Phenomenon

When a transformer is energized with a large amount of residual flux, the iron core is driven into deep saturation. The flux density is above the knee point of the B-H curve for large portions of each cycle, which makes the second harmonic content low [11]. Different residual flux conditions in Phase A are simulated in this section to verify the performance of the proposed method during ultra-saturation. Z_S is set as 5 Ω for long-lasting low second harmonic content. The knee voltage is set as 1.12 to drive the transformer into deep saturation more easily. The simulation results are listed in Table XI, which presents the values for the largest inrush currents. Fig. 15 shows the second harmonic contents of the $I_{1\mathrm{A}}$ and I_{dA} while the residual flux is 0.8 p.u. I_{dA} is the differential current of Phase A. The transformer experiences ultra-saturation during inrush, and the second harmonic content are below 15% after $t = 0.32$s. It can be seen from the figure that the Y-Δ transformation also contributes to the low second harmonic content. The main criterion works well under this condition, since the voltage drops will not exceed $\alpha_{\max}^{\mathrm{inrush}}$. The auxiliary criterion will also not misoperate due to the low differential power. In addition, if the transformer is energized on load, the proposed method may misoperate. The reason is that the ΔP of the secondary side during energization is not taken into consideration. Thus, the main criterion should be blocked. This is one limitation of the proposed scheme. However, energization of the transformer on load seldom happens in practice.

E. CT Saturation and Coupling Capacitor Voltage Transformer (CCVT) Measurement Errors

Internal faults with CT saturation are simulated in this section. Taking the Phase A-to-ground fault as an instance, currents in the transformer's primary side are shown in Fig. 16, and the FCDP is shown in Fig. 17. Although abnormal change of the data due to CT saturation causes errors in calculating the fault components of currents, the FCDP still exceeds the threshold during the CT saturation. The FCDP keeps reliable as in the non-saturation case.

In comparison, CT saturation during inrush due to large and long-lasting DC component is simulated, by setting the residual flux in the CT as 0.65 p.u. Currents in the transformer's primary side are shown in Fig. 18, and the FCDP is shown in Fig. 19. Although the FCDP contains errors due to CT Saturation, P_{fset}

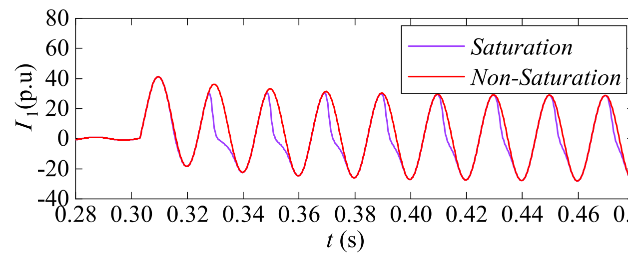

Fig. 16. Current of the Primary Side in Phase A During the Phase A-to-ground Fault.

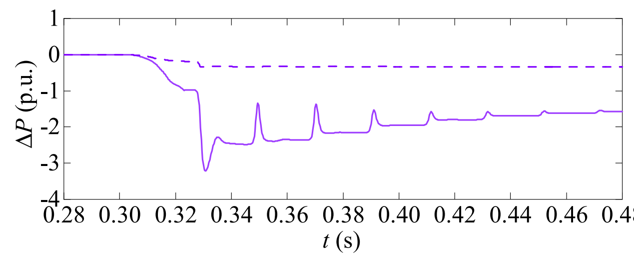

Fig. 17. FCDP During the Phase A-to-ground Fault with CT Saturation.

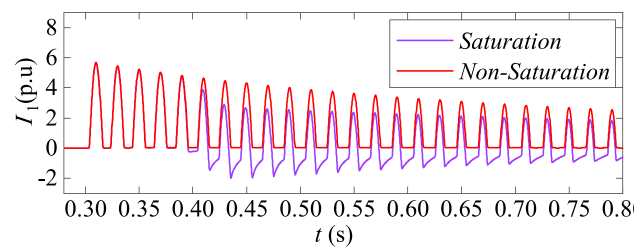

Fig. 18. Current of the Primary Side in Phase A During Inrush.

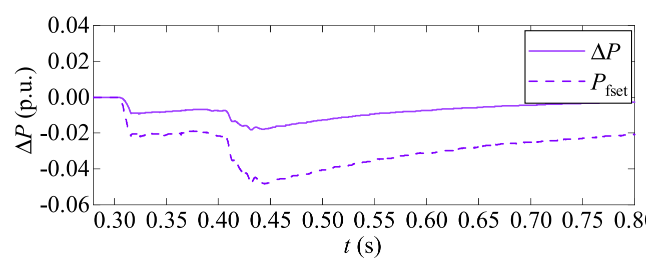

Fig. 19. FCDP During Inrush.

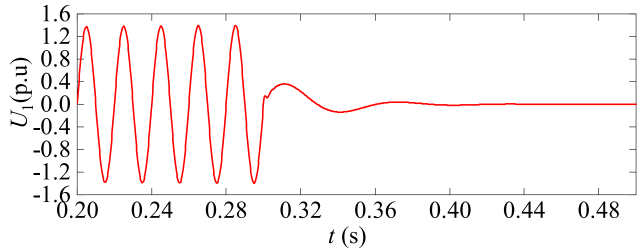

Fig. 20. CCVT Transients during Metallic Faults.

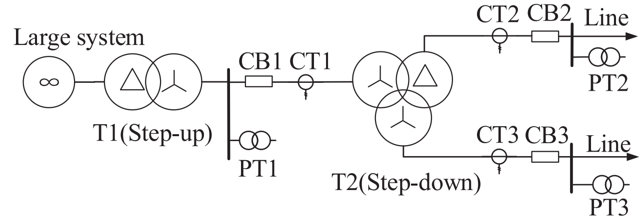

Fig. 21. Test System in the EPDL.

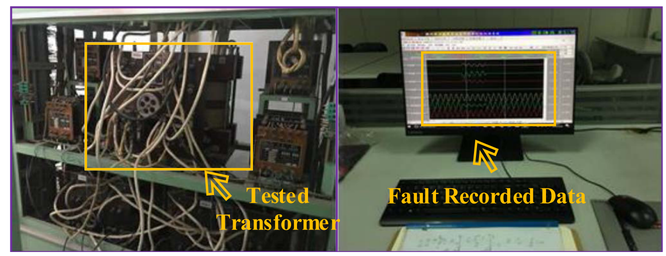

Fig. 22. Test Field in the EPDL.

also varies as the error changes. What makes a decision for the FCDP-based criterion is the voltage drop. The CT saturation has less influence on the FCDP-based criterion unless P_{fset} is limited to $P_{\mathrm{fset}}^{\max}$. The system impedance angle is used in (13), which will not change with the phase angle errors caused by CT saturation. To prevent the possible misoperation, a large K_{rel1} should be set for large inrush with CT saturation.

The voltage can be measured by the voltage transformer (VT) of the bus. If the scheme is used for a transformer whose main protection and backup protection are separated in different devices and thus the voltage data are not collected, the secondary cable or optical fiber should be installed between the VT and protection device. The VT can be a potential transformer (PT) or a coupling capacitor voltage transformer (CCVT). The latter may cause transients when large voltage drop occurs. The magnitude and phase angle errors will generate and affect the performance of the power differential protection. The CCVT transient during metallic phase-A-to-ground faults at F3 is shown in Fig. 20. The error is as large as 25% of the nominal voltage. If large transients occur during external faults, the proposed method may misoperate.

To solve the problem, two measures can be taken, including using CCVT with high sum of stack capacitances and pre-filtering the voltages using a filter designed specially to cope with CCVT transients. The higher the sum of the stack capacitances, the lower the magnitude of the transients [42]. However, the first measure will cause increased investment. At the same time, the trip time for the main criterion should be adjusted to one cycle later, which will slow down the speed of protection. Pre-filtering the voltages is a better choice. Modern microprocessor-based relays often incorporate techniques to deal with CCVT transients. For example, [43] provides a two-stage filter, with the ability of noise suppression and dynamic memory. By using a specially designed filter, less than 0.6% (of the nominal) transient errors due to the CCVT transients will be introduced. Then, the proposed method can work effectively.

F. Experiment in the EPDL

The test system constructed in the EPDL is shown in Fig. 21, and the test field is shown in Fig. 22. The tested transformer (step-down transformer) is connected to a no-load line. The voltage rating of the transformer is 1030 V/800 V/220 V. The system impedance is $8\Omega\angle 80^\circ$. $\alpha_{\max}^{\mathrm{inrush}} = 0.31$. Cases conducted in the EPDL include magnetizing inrush and faults at the secondary and tertiary windings.

TABLE XII
TEST RESULTS DURING INTERNAL FAULTS IN THE EPDL

Fault Location	Fault Type	ΔP(p.u.)	P_{fset}(p.u.)	P_{d}(p.u.)
Fault at secondary side	AG	−0.1059	−0.1013	0.0653
	AB	−0.1658	−0.1315	0.0565
	AC	−0.1691	−0.1357	0.0610
	ABG	−0.1865	−0.1413	0.0980
	ACG	−0.1797	−0.1379	0.0804
	ABC	−0.2971	−0.2064	0.1130
Fault at tertiary side	AB	−0.1912	−0.1595	0.1421
	AC	−0.1887	−0.1396	0.1727
	ABG	−0.2135	−0.1746	0.1339
	ACG	−0.2169	−0.1669	0.1701
	ABC	−0.3900	−0.2351	0.2816
Turn-to-turn fault	2.28%	–	–	0.1603
Energization with a fault at low-voltage side	AB	−0.1802	−0.1494	0.1553
Energization with turn-to-turn fault	2.28%	–	–	0.1324

Table XII describes the FCDPs and conventional differential powers. As presented in the table, the main criterion can recognize internal faults with or without inrush correctly, except a turn-to-turn fault with small short-circuit ratio. Nevertheless, sensitivity of the auxiliary criterion is high during the turn-to-turn fault. The proposed method can protect the tested transformer reliably during internal faults.

In addition, multiple tests of energization without faults are conducted. When RMS value of the inrush is 5.2 A, maximum absolute value of the FCDP is 23.25 W, which is much less than the threshold. This means the proposed method can distinguish internal faults from inrush reliably.

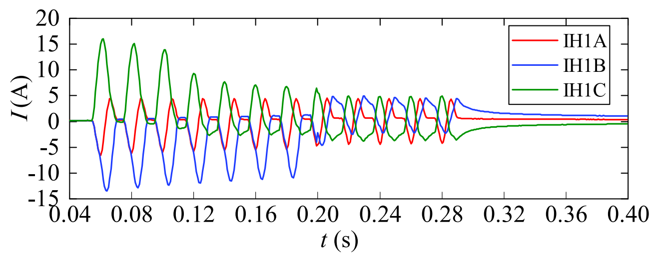

Fig. 23. Currents of the Transformer Primary Side Recorded in the Field.

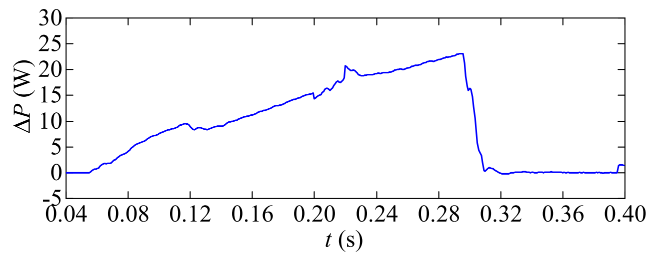

Fig. 24. FCDP Calculated by Actual Recording Data.

TABLE XIII
Comparative Assessment of the Proposed Method

Performance	WT	SDC	SCM	GDSC	Proposed Method
Asymmetrical faults detection	√	√	√	√	√
Symmetrical faults detection	√	×	×	√	√
Invulnerability to magnetizing inrush	√	√	√	√	√
Samples per cycle	256	80	512	256	24
Computation burden	High	Low	Low	Middle	Low

G. Actual Recording Data

Recording data of the actual power transformer protection device, which have been mentioned in Section I, are utilized to verify the reliability of the proposed method under energization. The power transformer is a YNyn0d11 transformer. The rated voltage and rated capacity are 230/121/38.5 kV and 180/180/90 MVA, respectively. The leakage reactance between the primary and secondary winding is 0.12 p.u, which is used to calculate P_{fset}. Sampling rate of the recording data is 1200 Hz. The differential current and second harmonic content has been shown in Fig. 1. Currents flowing through the primary side of the transformer are shown in Fig. 23. The calculated FCDP is positive, as shown in Fig. 24. Thus, the protection will not operate while the current differential protection operates in a false way. The actual inrush data can verify the reliability of the proposed method under energization.

H. Comparative Assessment

Performance assessment is carried out by comparing the proposed method with several existing methods. Table XIII lists the comparative study results with wavelet transform (WT) [18], superimposed differential current (SDC) [22], second central moment (SCM) [24] and generalized delayed signal cancelation (GDSC) [44]. SDC-based and SCM-based method cannot detect the three-phase faults. The WT-based and GDSC-based methods can detect different types of fault but require a high sampling rate. The proposed method can detect different types of faults with a low sampling rate, and its computation burden is low. 24 samples per cycle or 80 samples per cycle is commonly used in the practical protection device, which can meet the power calculation requirement. Thus, the proposed method is easy-to-implement in practice.

V. Conclusion

This article gives a whole energy perspective on the transformer and makes a new exploration on the power differential protection. A transformer protection scheme based on the FCN is proposed. The scheme focuses on the active power flowing to the transformer in the FCN, called FCDP. The polarity and magnitude of the FCDP is the key factor in internal fault identification. The FCDP is negative and large during internal faults, while it is positive or small during external faults and magnetizing inrush. Meanwhile, the negative effect of the DDC components can be significantly reduced using the differential DFT algorithm. In addition, the differential power based on the whole voltage and current components is used in the auxiliary criterion to improve sensitivity of the protection scheme under weak fault conditions. Simulations, experiments, and real-world recording data demonstrate the proposed scheme can distinguish internal faults from other conditions correctly. Furthermore, the scheme is not influenced by the magnetizing inrush during energization and voltage drop during faults. With little computation burden, the proposed scheme can protect the transformer reliably and is easy-to-implement in practice.

The proposed scheme has several limitations. The CCVT transients may lead to misoperation of the protection during external faults. Specially designed filter should be used to solve the problem. Meantime, if the transformer is energized on load in a few cases, the protection should be blocked to prevent the false trip. Besides, the maximum system impedance magnitude and the minimum impedance angle should be estimated for calculating P_{fset} where not available. This may decrease the sensitivity of the main criterion; nevertheless, the auxiliary criterion will work with high sensitivity under weak fault conditions. Additionally, due to the good performance under weak fault conditions, a better way of realizing the traditional power differential protection will be explored in the future work.

References

[1] IEEE Guide for Protecting Power Transformers, *IEEE Standard C37.91-2021 (Revision of IEEE Standard C37.91-2008)*, Jun. 2021.

[2] G. W. McKenna, "Theory and application of transformer differential protection," *Trans. Amer. Inst. Elect. Eng.*, vol. 69, no. 2, pp. 1197–1202, Jan. 1950.

[3] B. Kasztenny, M. Thompson, and N. Fischer, "Fundamentals of short-circuit protection for transformers," in *Proc. IEEE 63rd Annu. Conf. Protective Relay Eng.*, College Station, TX, USA, 2010, pp. 1–13.

[4] F. Naseri, Z. Kazemi, M. M. Arefi, and E. Farjah, "Fast discrimination of transformer magnetizing current from internal faults: An extended Kalman filter-based approach," *IEEE Trans. Power Del.*, vol. 33, no. 1, pp. 110–118, Feb. 2018.

[5] G. Baoming, A. T. de Almeida, Z. Qionglin, and W. Xiangheng, “An equivalent instantaneous inductance-based technique for discrimination between inrush current and internal faults in power transformers,” *IEEE Trans. Power Del.*, vol. 20, no. 4, pp. 2473–2482, Oct. 2005.
[6] J. L. Blackburn and T. J. Domin, *Protective Relaying: Principles and Applications*. Boca Raton, FL, USA: CRC Press, 2006.
[7] S. Krishnamurthy and B. E. Baningobera, “IEC61850 standard-based harmonic blocking scheme for power transformers,” *Protection Control Modern Power Syst.*, vol. 4, no. 2, pp. 121–135, 2019.
[8] A. M. Shah and B. R. Bhalja, “Fault discrimination scheme for power transformer using random forest technique,” *IET Gener. Transmiss. Distrib.*, vol. 10, no. 6, pp. 1431–1439, Apr. 2016.
[9] H. Dashti and M. Sanaye-Pasand, “Power transformer protection using a multiregion adaptive differential relay,” *IEEE Trans. Power Del.*, vol. 29, no. 2, pp. 777–785, Apr. 2014.
[10] Z. Lu, W. H. Tang, T. Y. Ji, and Q. H. Wu, “A morphological scheme for inrush identification in transformer protection,” *IEEE Trans. Power Del.*, vol. 24, no. 2, pp. 560–568, Apr. 2009.
[11] B. Kasztenny, M. J. Thompson, and D. Taylor, “Time-domain elements optimize the security and performance of transformer protection,” in *Proc. IEEE 71st Annu. Conf. Protective Relay Eng.*, College Station, TX, USA, 2018, pp. 1–15.
[12] X. Lin, J. Huang, L. Zeng, and Z. Q. Bo, “Analysis of electromagnetic transient and adaptability of second-harmonic restraint based differential protection of UHV power transformer,” *IEEE Trans. Power Del.*, vol. 25, no. 4, pp. 2299–2307, Oct. 2010.
[13] S. Hodder, B. Kasztenny, N. Fischer, and Y. Xia, “Low second-harmonic content in transformer inrush currents - analysis and practical solutions for protection security,” in *Proc. IEEE 67th Annu. Conf. Protective Relay Eng.*, 2014, pp. 705–722.
[14] R. P. Medeiros, F. B. Costa, K. M. Silva, J. D. J. C. Muro, J. R. L. Junior, and M. Popov, “A Clarke-wavelet-based time-domain power transformer differential protection,” *IEEE Trans. Power Del.*, vol. 37, no. 1, pp. 317–328, Feb. 2022.
[15] S. K. Murugan, S. P. Simon, and R. R. Eapen, “A novel signal localized convolution neural network for power transformer differential protection,” *IEEE Trans. Power Del.*, vol. 37, no. 2, pp. 1242–1251, Apr. 2022.
[16] E. C. Segatto and D. V. Coury, “A differential relay for power transformers using intelligent tools,” *IEEE Trans. Power Syst.*, vol. 21, no. 3, pp. 1154–1162, Aug. 2006.
[17] A. Wiszniewski and B. Kasztenny, “A multi-criteria differential transformer relay based on fuzzy logic,” *IEEE Trans. Power Del.*, vol. 10, no. 4, pp. 1786–1792, Oct. 1995.
[18] R. P. Medeiros and F. B. Costa, “A wavelet-based transformer differential protection: Internal fault detection during inrush conditions,” *IEEE Trans. Power Del.*, vol. 33, no. 6, pp. 2965–2977, Dec. 2018.
[19] A. Hooshyar, S. Afsharnia, M. Sanaye-Pasand, and B. M. Ebrahimi, “A new algorithm to identify magnetizing inrush conditions based on instantaneous frequency of differential power signal,” *IEEE Trans. Power Del.*, vol. 25, no. 4, pp. 2223–2233, Oct. 2010.
[20] H. Dashti, M. Davarpanah, M. Sanaye-Pasand, and B. M. Ebrahimi, “Discriminating transformer large inrush currents from fault currents,” *Int. J. Elect. Power Energy Syst.*, vol. 75, pp. 74–82, Feb. 2016.
[21] Z. Jiao and Z. Li, “Novel magnetization hysteresis-based power-transformer protection algorithm,” *IEEE Trans. Power Del.*, vol. 33, no. 5, pp. 2562–2570, Oct. 2018.
[22] A. M. Shah, B. R. Bhalja, and R. M. Patel, “New protection scheme for power transformer based on superimposed differential current,” *IET Gener. Transmiss. Distrib.*, vol. 12, no. 14, pp. 3587–3595, Aug. 2018.
[23] E. Ali, A. Helal, H. Desouki, K. Shebl, S. Abdelkader, and O. P. Malik, “Power transformer differential protection using current and voltage ratios,” *Elect. Power Syst. Res.*, vol. 154, pp. 140–150, Jan. 2018.
[24] H. Esponda, E. Vázquez, M. A. Andrade, and B. K. Johnson, “A setting-free differential protection for power transformers based on second central moment,” *IEEE Trans. Power Del.*, vol. 34, no. 2, pp. 750–759, Apr. 2019.
[25] A. Moradi and S. M. Madani, “Predictive formulas to improve transformer protection during inrush current using the proposed DC equivalent circuit,” *IEEE Trans. Power Del.*, vol. 35, no. 2, pp. 919–928, Apr. 2020.
[26] K. Yabe, “Power differential method for discrimination between fault and magnetizing inrush current in transformers,” *IEEE Trans. Power Del.*, vol. 12, no. 3, pp. 1109–1118, Jul. 1997.
[27] J. Huang, H. Gao, L. Zhao, and Y. Feng, “Instantaneous active power integral differential protection for hybrid AC/DC transmission systems based on fault variation component,” *IEEE Trans. Power Del.*, vol. 35, no. 6, pp. 2791–2799, Dec. 2020.
[28] M. Schuster and G. Herold, “Power based differential protection for three phase transformers,” in *Proc. PowerTech Conf.*, . 1999, Art. no. 204.
[29] F. Namdari, S. Jamali, and P. A. Crossley, “Power differential protection as primary protection of transmission lines and busbars,” in *Proc. IEEE Int. Conf. Develop. Power Syst*, 2008, pp. 80–85.
[30] P. Gawande and S. Dambhare, “Enhancing security of distance relays during power swing unblocking function for double circuit transmission lines: A differential power approach,” in *Proc. 13th Int. Conf. Develop. Power Syst*, 2016, pp. 1–6.
[31] H. A. Darwish, A.-M. I. Taalab, and E. S. Ahmed, “Investigation of power differential concept for line protection,” *IEEE Trans. Power Del.*, vol. 20, no. 2, pp. 617–624, Apr. 2005.
[32] X. Yin, D. Chen, Z. Zhang, and Y. Li, “Fault component based digital differential protection,” *Automat. Electric Power Syst.*, vol. 23, no. 11, pp. 13–17, Jun. 1999.
[33] F. Oechsle, K. Feser, N. Schuster, and L. Philippot, “Active power differential algorithm for protection of transmission lines,” in *Proc. PowerTech Conf.*, . 1999, Art. no. 207.
[34] J. Huang, H. Gao, F. Peng, and X. Liu, “Virtual active power differential protection for transmission lines,” *Automat. Electric Power Syst.*, vol. 41, no. 14, pp. 190–196, Nov. 2017.
[35] T. G. Bolandi, H. Seyedi, and S. M. Hashemi, “Protection of transmission lines using fault component integrated power,” *IET Gener. Transmiss. Distrib.*, vol. 8, no. 12, pp. 2163–2172, Dec. 2014.
[36] M. Nagpal, T. G. Martinich, A. Moshref, K. Morison, and P. Kundur, “Assessing and limiting impact of transformer inrush current on power quality,” *IEEE Trans. Power Del.*, vol. 21, no. 2, pp. 890–896, Apr. 2006.
[37] B. Zhang and X. Yin, *Power System Protective Relaying*. Beijing, China: China Electric Power Press, 2009.
[38] *Guide for Reactance Method to Detect and Diagnose Winding Deformation of Power Transformer*, DL/T 1093-2018, China, 2018.
[39] Y. A. Familiant, J. Huang, K. A. Corzine, and M. Belkhayat, “New techniques for measuring impedance characteristics of three-phase AC power systems,” *IEEE Trans. Power Electr.*, vol. 24, no. 7, pp. 1802–1810, Jul. 2009.
[40] C. Yao, Z. Zhao, Y. Mi, C. Li, Y. Liao, and G. Qian, “Improved online monitoring method for transformer winding deformations based on the Lissajous graphical analysis of voltage and current,” *IEEE Trans. Power Del.*, vol. 30, no. 4, pp. 1965–1973, Aug. 2015.
[41] X. Deng, J. Suonan, Z. Wang, and Z. Hou, “A novel busbar protection based on sequence component integrated impedance,” *Power Syst. Tech.*, vol. 35, no. 7, pp. 208–213, Jul. 2011.
[42] B. Kasztenny, D. Sharples, V. Asaro, and M. Pozzuoli, “Distance relays and capacitive voltage transformers – balancing speed and transient overreach,” in *Proc. 53rd Annu. Conf. Protective Relay Eng.*, College Station, TX USA, 2000, p. 9.
[43] B. Kasztenny and V. Asaro, “CVT transient filter,” U.S. Patent 6420875 B1, Jul. 16, 2002.
[44] Y. N. Batista, H. E. P. de Souza, F. D. A. D. S. Neves, and R. F. D. Filho, “A GDSC-based technique to distinguish transformer magnetizing from fault currents,” *IEEE Trans. Power Del.*, vol. 33, no. 2, pp. 589–599, Apr. 2018.

Fang Peng (Member, IEEE) was born in Hebei Province, China, in 1992. She received the B.Sc. degree in electrical engineering from the Hebei University of Technology, Tianjin, China, in 2012, and the Ph.D. degree in electrical engineering from Shandong University, Jinan, China, in 2018. She is currently a Postdoctor with the School of Electrical Engineering, Shandong University, Jinan, China. Her research interests include power system simulation, transformer protection, and protection technology of power system with high-penetration renewables.

Houlei Gao was born in Shandong Province, China, in 1963. He received the B.Sc. and M.Sc. degrees in electrical power engineering from Shandong University, Jinan, China, in 1983 and 1988, respectively, and the Ph.D. degree from Tianjin University, Tianjin, China, in 1997. From 2004 to 2005, he was with the School of Electrical and Electronic Engineering, Queen's University Belfast, Belfast, U.K. He is currently a Professor with the School of Electrical Engineering, Shandong University. His research interests include power system protection, feeder automation, distributed generation and digital substation.

Jiakai Huang was born in Shandong, China, in 1992. He received the B.S. degree in power system and its automation, and the Ph.D. degree in electrical engineering from Shandong University, Jinan, China, in 2015 and 2021, respectively. He is currently an Engineer with Electric Power Research Institute, State Grid Tianjin Electric Power Company, China. His research interests include power system fault analysis and protection.

Yifei Guo received the B.E. and Ph.D. degrees in electrical engineering from Shandong University, Jinan, China, in 2014 and 2019, respectively. He is currently a Lecturer with the School of Engineering, University of Aberdeen, Aberdeen, U.K. During 2019–2022, he was a Postdoctoral Research Associate with the Department of Electrical and Electronic Engineering, Imperial College London, London, U.K., and the Department of Electrical and Computer Engineering, Iowa State University, Ames, IA, USA. His research interests include power system modeling, control and optimization. Dr. Guo is an Assistant Editor for *International Journal of Electrical Power & Energy Systems* and a Young Editor for *Applied Energy*.

Yiqing Liu was born in Shandong, China. He received the B.Sc. and M.Sc. degrees in electrical engineering from Tianjin University, Tianjin, China, in 2000 and 2003, respectively, and the Ph.D. degree in electrical engineering from Shandong University, Jinan, China, in 2012. He is currently a Professor with the School of Electrical Engineering, University of Jinan, Jinan, China. His research interests include relay protection in active distribution network and relay protection for distributed generation.

Yongfeng Zhang received the Ph.D. degree in electrical engineering from Tianjin University, Tianjin, China, in 2017. He is currently an Associate Professor of electrical engineering with the School of Electrical Engineering, University of Jinan, Jinan, China. His technical research interests include stability regions of general nonlinear dynamical systems, global and robust optimization techniques, and their practical applications to power systems.